

Magnetoacoustic position imaging for liquid metal in animal interstitial structure

Xiao-He Zhao(赵筱赫), Guo-Qiang Liu(刘国强), Hui Xia(夏慧), Yan-Hong Li(李艳红)
Citation: Chin. Phys. B . 2020, 29(5): 054305 . **doi:** 10.1088/1674-1056/ab8207
Journal homepage: http://cpb.iphy.ac.cn; http://iopscience.iop.org/cpb

What follows is a list of articles you may be interested in

Lorentz force electrical impedance tomography using pulse compression technique

Zhi-shen Sun(孙直申), Guo-qiang Liu(刘国强), Hui Xia(夏慧)
Chin. Phys. B . 2017, 26(12): 124302 . **doi:** 10.1088/1674-1056/26/12/124302

Ultrasound-mediated transdermal drug delivery of fluorescent nanoparticles and hyaluronic acid into porcine skin *in vitro*

Huan-Lei Wang(王焕磊), Peng-Fei Fan(范鹏飞), Xia-Sheng Guo(郭霞生), Juan Tu(屠娟), Yong Ma(马勇), Dong Zhang(章东)
Chin. Phys. B . 2016, 25(12): 124314 . **doi:** 10.1088/1674-1056/25/12/124314

Magnetic interaction in the metamaterial/magnet system

M. K. Alqadi, F. Y. Alzoubi
Chin. Phys. B . 2014, 23(8): 087506 . **doi:** 10.1088/1674-1056/23/8/087506

Magnetoacoustic position imaging for liquid metal in animal interstitial structure*

Xiao-He Zhao(赵筱赫)[1,2], Guo-Qiang Liu(刘国强)[1,2,†], Hui Xia(夏慧)[1,2], and Yan-Hong Li(李艳红)[1,2]

[1] *Institute of Electrical Engineering, Chinese Academy of Sciences, Beijing* 100190, *China*
[2] *University of Chinese Academy of Sciences, Beijing* 100049, *China*

(Received 9 January 2020; revised manuscript received 13 February 2020; accepted manuscript online 23 March 2020)

Magnetoacoustic tomography with magnetic induction (MAT-MI), as a new kind of *in-vivo* imaging method, has potential application value in interstitial fluid research. In this paper, we propose the application of MAT-MI with liquid metal serving as a tracer of the interstitial structure to study its fluid behavior, and use it to implement the positional imaging of the spatial distribution of liquid metal. Owing to the particularity of liquid metal magnetoacoustic pressure (MAP) signals, we propose an envelope analysis method to extract the rising edge of the amplitude envelope of the detected waveform as effective position data. And for the first time, we propose the method of superpositing pixel matrix to achieve the position imaging of liquid metal. Finally, the positional imaging of the liquid metal sample embedded in the gel is achieved to have relatively accurate results. This study provides a method of effectively extracting data and implementing the position imaging for liquid metal in the interstitial structure in the frame of MAT-MI.

Keywords: magnetic acoustic tomography with magnetic induction (MAT-MI), liquid metal, interstitial structure, position imaging

PACS: 43.80.+p, 72.55.+s, 73.50.Rb, 75.90.+w **DOI:** 10.1088/1674-1056/ab8207

1. Introduction

With the in-depth understanding of the life soft materials, the study of the interstitial structure as a new organ has gradually gained more and more attention. Since De Gennes PG used the concept of "soft matter" for the first time at the Nobel Prize Conference in 1991,[1] several teams worldwide have devoted to the research actively on interstitial structures and their fluid behaviors, trying to reveal the operation law of the interstitial fluid and establish a perfect model describing the life fluid operation system. Preliminary studies have shown that the interstitial structures form a highly efficient communication framework for organisms. The interstitial fluid circulates under the framework to achieve efficient long-distance transport of biological material, energy, and information, the operational characteristics of which are closely related to physiological and pathological conditions and can comprehensively reflect a variety of information about the status of living organisms.[2,3] At present, researchers mainly observe the morphology and distribution characteristics of interstitial structures through anatomical methods,[4–6] which cannot investigate the fluid behavior under living conditions. Fluorescent tracer is an ideal medium for investigating fluid behavior[7,8] and has been widely used in biological fluid pipeline angiography. However, the short development time of fluorescence restricts its application in interstitial fluid research, since the interstitial fluid has a large spatial scale cycle over a large period with the development of new materials. Researchers explore the nanoparticles used as markers to study the behavior of interstitial fluids and obtain initial progress.[9] *In-vivo* imaging methods have the characteristics of not destroying the life state of living organisms and are an effective method of studying the macroscopic structure and fluid behavior of interstitial tissues. For the physical characteristics of interstitial tissues, imaging methods widely used in disease diagnosis, such as ultrasound, CT, *etc*., have their limitations in the study of interstitial structures and fluid behavior. For example, the contrast of ultrasound imaging is low for the small difference in acoustic impedance between normal interstitial structures and its adjacent tissue, while CT has the risk of ionizing radiation. The magnetic resonance imaging (MRI) is a new type of *in vivo* imaging technique with high contrast and good resolution. In recent years, with the in-depth research on functional Magnetic Resonance Imaging (fMRI), the MRI has the function of tracking and imaging the moving fluids.[10] However, MRI equipment is generally bulky and has strict requirements for environmental electromagnetic parameters in its working area, which restricts its application in clinical monitoring of interstitial fluid that moves continuously over a large time span all over the body. Therefore, it is necessary to develop an *in-vivo* imaging method for the interstitial structure, which can achieve long-term clinical monitoring of interstitial fluid characteristics and systematically study the intersti-

*Project supported by the National Natural Science Foundation of China (Grant Nos. 61771448, 61427806, and 51937010), the National Key Research and Development Program of China (Grant No. 2018YFC0115200), and the Natural Science Fund from the Chinese Academy of Sciences (Grant Nos. ZDKYYQ20190002 and YJKYYQ20190005).

†Corresponding author. E-mail: gqliu@mail.iee.ac.cn

© 2020 Chinese Physical Society and IOP Publishing Ltd

tial fluid behavior.

MAT-MI, as a new type of *in-vivo* imaging technique, is sensitive to conductivity parameters and has the characteristics of no-radiation, no-contacting, and its imaging that is not restricted by the physical structure of tissues. Since Xu and He from University of Minnesota (USA) proposed the technology of MAT-MI in 2005,[11] researchers have done a lot of work on early tumor detection based on the conductivity difference between normal and diseased tissues, and have achieved a series of results in theoretical research, experimental platforms, and imaging algorithms.[12] Based on the analytical model and the finite element calculation model, the researchers conducted numerical analysis and established a mathematical and physical model of the system.[13–16] Researchers fully demonstrated the parameters of the experimental system and established an experimental platform. On the basics of this, they achieved the experimental studies of physical phantoms and biological tissues, which demonstrated the feasibility and performance of MAT-MI.[17–20] In recent years, the researchers have gradually improved the imaging algorithm to make it more suitable for clinical applications.[21,22] In tumor detection, the conductivity of the lesion area is abnormal and the distribution is unknown. It is necessary to reconstruct the conductivity of the target area and its spatial distribution based on the detected magnetoacoustic (MA) signal and take this as a reference to discriminate and divide the cancerous area.[21–24] Therefore, it requires relatively high spatial resolution and accuracy of reconstructed conductivity of the abnormal area. In the cancer detection in MAT-MI, the demagnetization effect of the induced current can be neglected in the electromagnetic field analysis, and the biological tissue is reduced to a one-way coupled electromagnetic model due to the low conductivity of biological tissues themselves (< 1 S/m). At the same time, the acoustic impedance difference between tissues is usually ignored, and it is regarded as an acoustic uniform fluid, since the acoustic characteristics of the biological tissue including the cancerous area are no more than 10%, which is much smaller than the electrical conductivity difference ($> 100\%$). In the reconstruction algorithm, the unknown conductivity of the tissue is taken as the target parameter. The MA source distribution is reconstructed from the detected MAP of the sample points on the scanning path, and then the spatial distribution of the electrical conductivity is calculated and the precise boundary is reconstructed, which was taken as the reference for cancer screening and its boundary division.

However, in the study of interstitial structure, due to the absence of electrical conductivity abnormal areas of the lesions, the electrical conductivity difference of normal tissues in various parts of the organism is relatively small, which results in the fact that the MA signal is too weak to detect. In order to solve this problem, Zhao *et al.* proposed the idea of studying the interstitial structure and fluid behavior by using gallium-based liquid metal with high conductivity as the marker and measurement medium in the MAT-MI detection.[25] Galinstan (Quality ratio: Ga : In : Sn = 62.5 : 21.5 : 16) is one kind of gallium-based liquid metal that has good chemical stability and good biocompatibility. Its melting point is -18 °C and has good fluidity and low viscosity at room temperature (as shown in Fig. 1(a)), which makes it possible to directionally flow through the animal's interstitial fluid channels. Shown in Fig. 1(b) is a typical liquid metal distribution in the interstitial structure of mouse forelimbs.[27] In MAT, we can approximate biological tissue as a non-conductive material, and attribute the problem to solving the spatial distribution of liquid metal without solving its conductivity value, since the conductivity of liquid metal is already known (6.4×10^6 S/m) and much larger than that of biological tissue (< 1 S/m). According to the characteristics of the interstitial structure, liquid metal is distributed in a curve or a sheet-like or hollow tubular shape with a small cross-section over a large spatial scale.[2–6] Therefore, we only care about the spatial orientation of the liquid metal and the connectivity values of the various parts without accurately depicting the boundary shape of the liquid metal. According to this, in this paper we propose a position imaging method for liquid metal in the interstitial structure by using the MA–MI detection, which has high fault tolerance ("fault tolerance" is widely used in the engineering field to describe the system's ability to operate under partial fault conditions. This concept in the present article is cited from the literature to indicate the performance of the system for normal imaging when some sampling units fail or are incorrectly sampled) and robustness for its advantage of avoiding the problem that the unsolved inequalities are caused by data corruption. The envelope analysis method is employed to extract liquid metal position information and generate normalized position sequences, and a geometric imaging algorithm based on the pixel matrix superposition was designed to achieve positional imaging of the liquid metal on different slices. The result indicated that this imaging method has relatively low dependence on the number of sampling points, small amount of computation, high computing speed, which can achieve online position imaging of the liquid metal distribution in the interstitial structure.

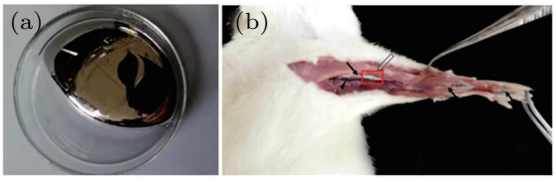


Fig. 1. Pictures of galinstan (quality ratio: Ga : In : Sn = 62.5 : 21.5 : 16) for (a) liquid metal in air at room temperature,[26] and (b) galinstan's distribution in fascial space of mice forelimb (black solid arrow).[27]

2. Signal processing and position imaging algorithm

2.1. Principle of ma detection for liquid metal

The schematic diagram of the MAT-MI detection system for liquid metal in the interstitial structure is shown in Fig. 2. Liquid metal is distributed continuously in the space of the biological interstitial structure, which was placed in a complex magnetic field combined with a static magnetic field $\boldsymbol{B}_0$ and a pulsed magnetic field $\boldsymbol{B}(t)$ which was generated by a pair of Helmholtz coils with pulsed current $I(t)$. Under the excitation of $\boldsymbol{B}(t)$, an induction current whose density is expressed as $\boldsymbol{J}(\boldsymbol{r},t)$ was generated in the liquid metal. The Lorentz force generated by the current subjected to in the magnetic field excited a sound wave which was detected by ultrasonic transducers located around the sample. In the experiment, considering the penetration depth of the tissue and the spatial resolution of the acoustic wave, the MA system is generally excited by a pulsed current with 1 μs in width, and the ultrasonic transducer with a center frequency of 1 MHz is employed to receive the sound field signal.

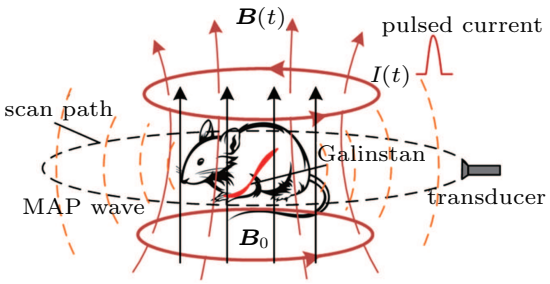


Fig. 2. Principle of MAT-MI for liquid metal in interstitial structure.

Taking into account the differences in physical properties between materials, the wave equation of acoustic pressure p can be expressed in the following form:

$$\frac{1}{\rho c^2}\frac{\partial^2 p(\boldsymbol{r},t)}{\partial^2 t}-\nabla\cdot\left(\frac{1}{\rho}\nabla p(\boldsymbol{r},t)\right)=-\nabla\cdot\frac{1}{\rho}[\boldsymbol{J}(\boldsymbol{r},t)\times\boldsymbol{B}]. \quad (1)$$

There are two kinds of fluids, *i.e.*, liquid metal and biological tissue in the MA system. In Eq. (1), ρ is the bulk density of the fluid, which is 1000 kg/m^3 and 6400 kg/m^3 of the biological tissue and the liquid metal respectively, and c is the acoustic propagation velocity in the fluid, which is 1500 m/s and 2000 m/s of the biological tissue and liquid metal, respectively. $\boldsymbol{B}=\boldsymbol{B}_0+\boldsymbol{B}(t)$ is the flux density of the complex magnetic field, and the static magnetic field $\boldsymbol{B}_0$ is usually much larger than the amplitude of the pulsed magnetic field $\boldsymbol{B}(t)$ to ensure the safety of the biological tissue under the pulsed magnetic field, that is $\boldsymbol{B}\approx\boldsymbol{B}_0$. The effect of induced current in the tissue can be ignored since the conductivity of liquid metal (3.8×10^6 S/m) is much larger than that of biological tissue (<1 S/m). The induced current density of the liquid metal exhibits a strong demagnetization effect under pulse excitation, which is quite different from that in biology tissue with low conductivity. The skin depth of the liquid metal is about 0.2 mm which is much smaller than the acoustic wavelength in liquid metal under the MAP detection frequency. As a result, the induction current can be equivalent to the surface current on the outer surface of the liquid metal, which can be expressed as $\boldsymbol{J}_{\partial\Omega_2}$, where $\partial\Omega_2$ indicates the outer boundary of liquid metal region. Equation (1) is expanded as follows:

$$\begin{aligned}&\frac{1}{c^2}\frac{\partial^2 p(\boldsymbol{r},t)}{\partial^2 t}-\nabla^2 p(\boldsymbol{r},t)\\&=-\nabla\cdot[\boldsymbol{J}_{\partial\Omega_2}\times\boldsymbol{B}]-\rho\nabla\frac{1}{\rho}\cdot\left[\left(\boldsymbol{J}_{\partial\Omega_2}\times\boldsymbol{B}\right)+\nabla p(\boldsymbol{r},t)\right]. \quad (2)\end{aligned}$$

It can be seen from the right-hand side of Eq. (2) that in addition to the Lorentz force source term, the sound source also includes the secondary component related to fluid density difference. In biological tissue imaging, the sound source of this type is zero because the density difference between tissues is not considered. However, in the MA process of biological tissue containing liquid metal, the density difference cannot be ignored. Therefore, it is necessary to consider the secondary sound source term due to the density difference, which makes the MA component more complicated, and its data extraction and imaging algorithm are quite different from those involved in biological tissue imaging.

2.2. Envelope analysis method

The MA signal characteristics of liquid metal in biological tissues are significantly different from those in cancer detection because the electromagnetic properties and acoustic properties of liquid metals are quite different from those of biological tissues. Zhao *et al.* studied the MA signal characteristics of liquid metals with different sizes under a certain symmetrical simplification framework based on the background of MAT-MI, and provided a theoretical basis for the position information extraction of liquid metal.[16] According to the distribution characteristics of liquid metal and the magnetic field distribution of the imaging area, the shape of any slice can be regarded as having a certain symmetry. Therefore, the characteristics of induced current and MAP still satisfy the symmetry relationship described in Ref. [25].

According to the research by zhao *et al.*, the original acoustic wave and the reflected ones coexist due to the reflection and incomplete projection of acoustic waves at the interface between liquid metal and tissue, which results in complex acoustic signal components detected by the transducer at the sampling point. In addition, there are large differences in the detection waveforms of the MAP of liquid metal with different sizes embedded in tissues, which makes it difficult to extract the location information of the liquid metal. In experiment, a narrow-band ultrasonic transducer was usually employed to

detect MAP signals. The transducer output waveform is a typical narrowband signal, which can be expressed as follows:

$$s(t) = A(t)\cos(2\pi f_0 t + \phi(t)), \tag{3}$$

where $\phi(t)$ is the phase time function and $A(t)$ is the amplitude time function, which is the envelope of the oscillating function when its equivalent frequency is much smaller than the main frequency f_0 of the function. According to the Hilbert transform principle, $A(t)$ can be obtained from the following formula:

$$A(t) = \sqrt{s^2(t) + \hat{s}^2(t)}, \tag{4}$$

where $\hat{s}(t) = s(t) \times 1/\pi t$, which is the Hilbert transform of $s(t)$.

According to Ref. [16], when the size of liquid metal is relatively large, the MAP envelope has multiple peaks, and the first two peaks indicate the two boundaries of the liquid metal along the acoustic wave propagation path, which can be directly extracted to generate a normalized position sequence. Furthermore, the ratio between the amplitudes of the first two peaks on the envelope is 0.55, which is determined by the difference in acoustic impedance between the liquid metal and the biological tissue. The ratio can be expressed as $K = 1/(1 + r_p)$, where r_p is the reflection coefficient of sound pressure propagating from liquid metal to biological tissue. In this case, the positions of the first two peaks on the envelope can be directly extracted as the boundary information on both sides of the liquid metal. As the size of the liquid metal becomes smaller, the time interval between the MAP waveforms on the two sides of the boundaries decreases, and the waveform overlap gradually increases. When the first peak on the envelope is under the rising edge of the second cluster of waveform envelopes, the two sides of the liquid metal cannot be identified by the envelope. In this case, we need a new algorithm for boundary recognition. When the size of liquid metal is smaller than the half acoustic wavelength in liquid metal under the detection frequency, the detection signal has only one wave cluster due to the waveforms of the two boundaries on both sides almost completely overlapping and the peak of its envelope indicates the position of the liquid metal. In this condition, we will not be able to accurately extract the boundaries on both sides of the liquid metal, but we can extract the position information of the liquid metal by detecting the waveform. Furthermore, under this situation, the liquid metal in the interstitial structure can be attributed to the identification of small targets on a large spatial scale, and our task is to find their spatial location. Taking a cylindrical liquid metal sample with a diameter of 3 mm for example, the typical magnetic acoustic waveform of the transducer t on one slice is shown in Fig. 3(a). The effective signal detected by the transducer is one cluster of complex waveform. The red line in Fig. 3(b) is the envelope of the detected signal extracted by Hilbert transform. According to the previous analysis, the front boundary of the liquid metal is located 0.55 times of amplitude on the rising edge of the envelope. Therefore, extracting the corresponding data of the rising edge of the envelope and normalizing it, we can obtain a time sequence of liquid metal and biological tissue in the opposite direction to the acoustic wave propagation path as the red line shown in Fig. 3(c). In the sequence, "0" means the biological tissue, and "1" indicates the liquid metal. The spatial distribution of liquid metal and biological tissue on the acoustic path can be obtained by substituting the acoustic wave propagation velocity into the two media and converting the time axis into position information as shown in Fig. 3(d), where R_f and R_b indicate the distances from the two sides of the liquid metal to the transducer, respectively.

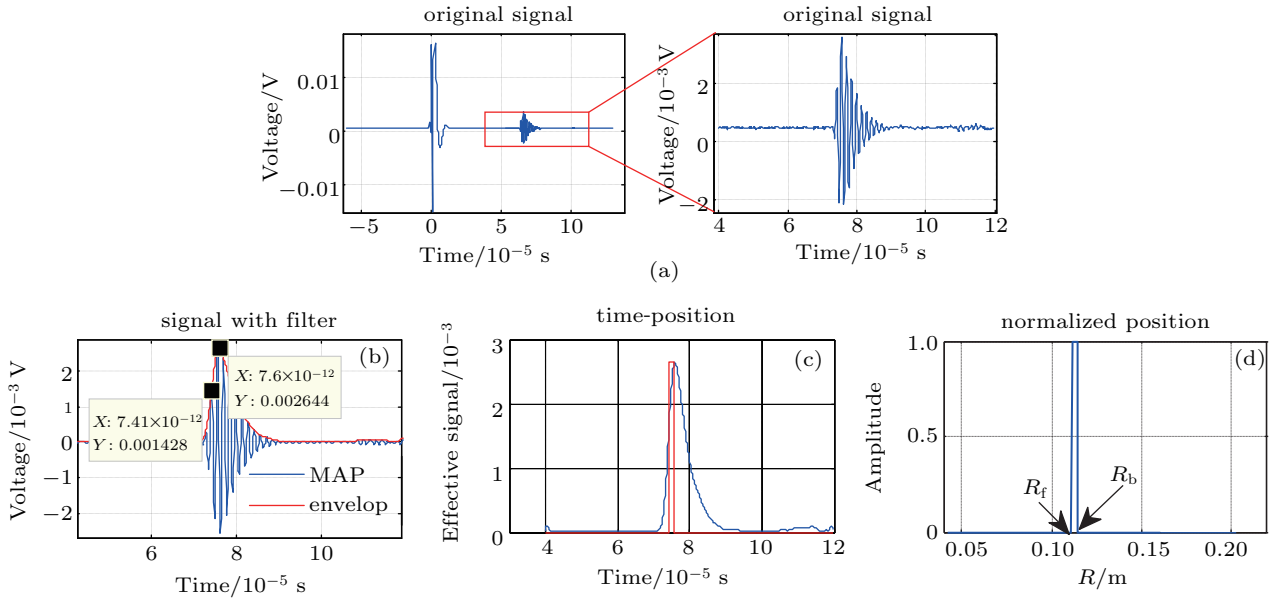


Fig. 3. Progress of MA signal processing and location information extraction, showing (a) original MAP signal, (b) envelope of signal with filter, (c) effective signal extraction of envelope, and (d) normalized position sequence on sound path.

2.3. Position imaging algorithm

According to the above analysis, the distance between the transducer and the liquid metal front and between the transducer and the back interface are $R_{\rm f}$ and $R_{\rm b}$ respectively. In the Cartesian coordinate system, when the coordinate of the transducer is $(x_{\rm t}, y_{\rm t})$, the possible regional coordinates of the liquid metal satisfy the following inequality if the directivity of the transducer is not considered:

$$R_{\rm f}^2 \leqslant (x-x_{\rm t})^2+(y-y_{\rm t})^2 \leqslant R_{\rm b}^2. \tag{5}$$

That is, when the liquid metal is distributed in any part of the arc-shaped region centered on $(x_{\rm t}, y_{\rm t})$ and the radius satisfies $R_{\rm f} \leqslant R \leqslant R_{\rm b}$ as shown by the gray area 1 in Fig. 4, the transducer can detect the MAP signal of Fig. 3(a). According to the geometric principle, more gray areas like 1 are needed to determine the position of the liquid metal. The intersection of all gray areas is as shown in Fig. 4 is the distribution area of liquid metal.

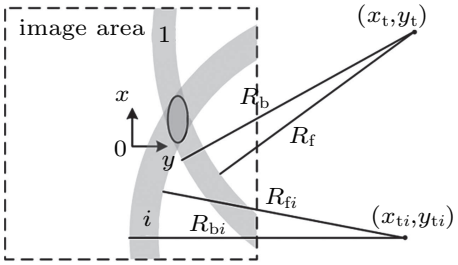


Fig. 4. Position imaging schematics.

In the MA image reconstruction, it is necessary to detect sound pressure data through multiple sampling points to achieve the reconstruction of target parameters. In the experiment, multi-point MAP data are sampled through single transducer scans according to a certain regular motion, or transducer array consisting of multiple detection units. If the number of sampling points is n and the position of each sampling point is known as (x_{it}, y_{it}), $i = 1,2,3,\ldots,n$ respectively, the inequality group with n inequalities can be established as follows according to formula (5):

$$R_{fi}^2 \leqslant (x-x_{ti})^2+(y-y_{ti})^2 \leqslant R_{bi}^2, \quad i=1,2,3,\ldots,n. \tag{6}$$

The liquid metal region is the solution of inequalities in formula (6).

In multiple points' sampling, the data quality of some sampling points is relatively poor or invalid sampling for various reasons, which will result in no solution to the inequality group. In order to avoid this problem, in this paper proposed is a method of implementing layer-by-layer superposition of pixel matrix for position imaging. The imaging region is divided into $m \times n$ pixel units, and a pixel matrix A_i $(i = 1,2,3,\ldots,n)$ of $m \times n$ is defined for each sample point. When the imaging region position (x, y) satisfies formula (6), the corresponding element in the pixel matrix is set to be 1, otherwise 0. That is, for each sampling point, the gray curved band in Fig. 3 is set to be 1, and the rest is set to be 0. The pixel matrix of all sampling points is superimposed layer by layer to obtain the total pixel matrix as follows:

$$A = \sum_i A_i \quad (i = 1,2,3,\ldots,n). \tag{7}$$

The liquid metal region is the area with the maximum value in the pixel matrix. Theoretically, the value of the liquid metal region in the pixel matrix should be equal to the number of sampling points. In multiple points' scanning, the strength of the MAP at some sampling points may be too small to be extracted from the system noise, which will lead to failing in effective signal extraction. It can prove that as long as more than 50% of effective sampling can be guaranteed, the positional imaging of liquid metal can be achieved by the pixel matrix superposition method. This method greatly improves the fault tolerance and robustness of the position imaging system.

3. Rotating scanning experiment and position imaging

3.1. Experimental system

In order to prove the analysis results above, we built an circle scanning MA detection system for experiment as shown in Fig. 5(a), in which the static magnetic field was provided by two pieces of NdFeB permanent magnet magnetized along the z direction to produce a uniform magnetic field $\boldsymbol{B}_0$ with a magnetic flux density of about 0.2 T along the z direction in the sample area. The pulsed current with the waveform as shown in Fig. 5(a) in the Helmholtz coil to generate a pulsed magnetic field $\boldsymbol{B}(t)$, which has the same direction as $\boldsymbol{B}_0$. Water was used as an acoustic coupling agent, and piezoelectric acoustic transducer with the impulse response waveform as shown in Fig. 5(a) was employed to receive MA signals. The liquid metal was poured into a soft rubber tube with an inner diameter of 3 mm and sealed at both ends, tilt-embedded in the gel as a test sample to simulate the distribution of liquid metal in the interstitial structure in the organism as shown in Fig. 5(b). Take 4 slice planes and scan them separately, then the distance between adjacent layers will be 10 mm. The scanning path of the sample and the transducer on each slice plane is shown in Fig. 5(c). The center of the circular scanning motion is taken as the ordinate origin. At each slice plane, the center coordinates of the liquid metal are (15, −4), (8, −4), (3, −4), and (−6, −5) (in unit mm) respectively. Taking the positive half-axis of the x axis as the starting position of the rotational scan, the transducer rotates counterclockwise along a circle with a radius R of 9.5 cm in steps of 5° (angle $\mathrm{d}\varphi$) and the total number of sample points n is 72.

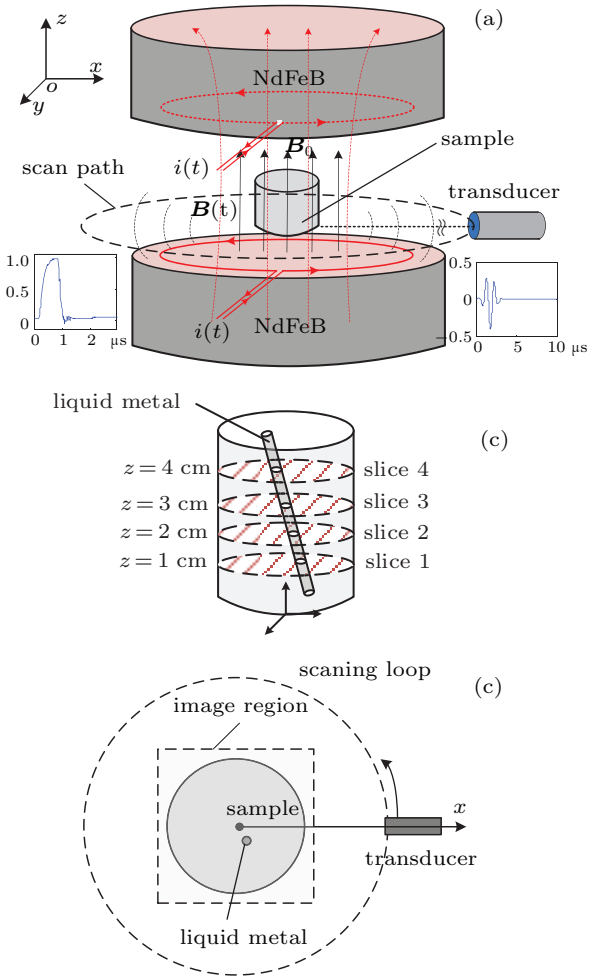


Fig. 5. Experimental system diagram, showing (a) structure of experimental system, (b) sample schematics, (c) scanning process in one slice.

3.2. Position imaging

The imaging area is a square with a side length of 4 cm, and its center is at the ordinate origin as shown in Fig. 4(c). According to the structure of the rotating scanning system, the coordinates of each sampling point position are as follows:

$$\begin{cases} x_{ti} = R * \cos(i\mathrm{d}\varphi), \\ y_{ti} = R * \sin(i\mathrm{d}\varphi), \end{cases} \quad i = 1, 2, 3, \ldots, n.$$

The imaging area was divided into 200×200 pixel units. As shown in Fig. 6(a), the position of each layer was imaged, and the maximum area in each layer was an approximately circular shape with a diameter of about 3 mm, and the central coordinates are (15.4, −3.2), (8.4, −4.2), (3, −4.4), (−6.2, −4.8) (in unit mm), respectively, which was substantially consistent with the position of the liquid metal in the test sample. This result shows the feasibility of extracting the rising edge of the amplitude envelope as a positional imaging parameter. According to the position imaging scheme, the maximum value of the pixel matrix should be equal to the total number of sampling points "n". However, the maximum values of the pixel matrix in the figures are all smaller than "n". This is because the failure of location data extraction due to poor signal-to-noise ratio at some sampling points. This also indicates that partial sampling data failure does not affect the imaging results, and the system has relatively high fault tolerance and robustness. The normalization liquid metal position images are shown in Fig. 6(b). Shown in Fig. 7(a) is the comparison of the position image of each layer with the original target position image, indicating that there is good overlap between the original position of the liquid metal and the imaging position. The coordinates of the imaging center points of each layer are extracted and compared with that of the center point of sample in each layer. The results indicate that there is good consistency between the position imaging results and the sample coordinates as shown in Fig. 7(b). The spatial orientation of liquid metal can be reconstructed through the information about each layer position.

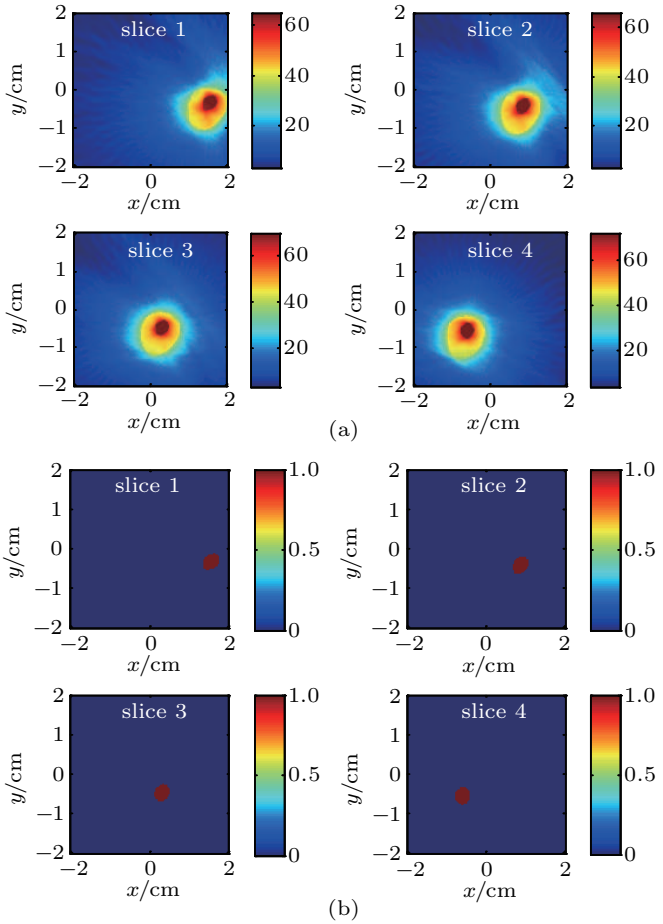


Fig. 6. Results of position imaging, showing (a) results of position imaging for each slice and (b) normalized position for each slice.

For liquid metal in biological tissues, the conductivity is a known parameter, and the target of imaging is to determine the spatial orientation of the liquid metal without concerning the specific shape of its boundary. So the goal of imaging for each slice is to answer the questions about liquid metal: "yes" or "no", and "where it is". Therefore, the number of sampling points can be appropriately reduced to simplify the imaging algorithm and improve the imaging efficiency. The liquid metal position images of 9 sampling points are uniformly arranged

on the scanning path as shown in Fig. 8, which indicates that the position reconstruction of the liquid metal can be realized by appropriately reducing the number of sampling points, and has a certain fault tolerance performance. It can prove mathematically that the position of the liquid metal region can be determined by at least three sequences of effective spatial positions of the sampling points.

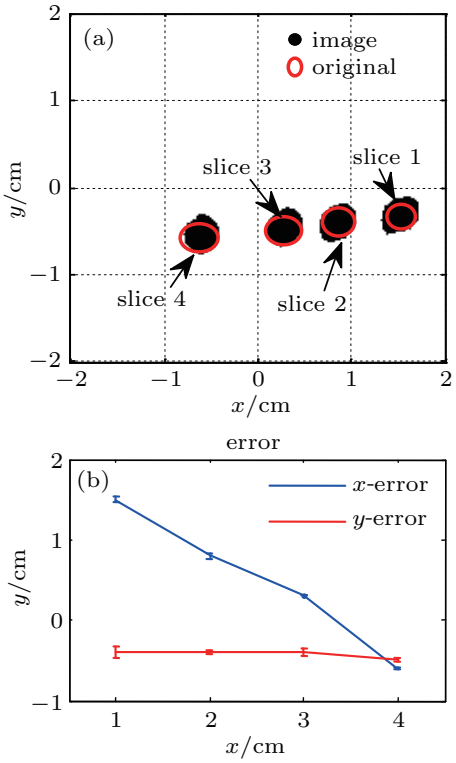


Fig. 7. (a) Comparison between position image and original target position for each layer, and (b) error analysis of imaging center coordinate).

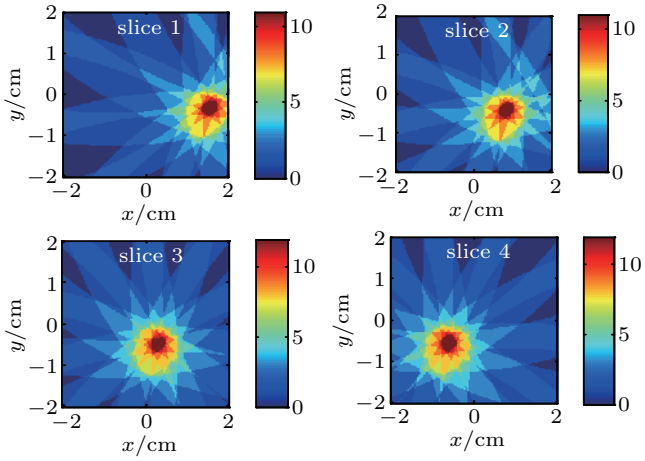


Fig. 8. Position reconstruction of liquid metal with fewer sampling points.

The method has potential application value in high-speed dynamic positioning detection of liquid metal for its advantages of small data volume, high calculation speed, and online imaging. At the same time, in the parallel detection system using a transducer array, there are fewer requirements for the number of detection units, which is convenient for system installation and integration.

The above results show that the imaging method proposed in this paper can achieve the position imaging of simple targets. In order to verify the universal applicability of the method, we performed this imaging method on a complex planar curved target, which injects liquid metal into the gel channel as shown in Fig. 9(a). Based on the data of 36 sampling points evenly distributed along the scanning circle, the position imaging results are shown in Fig. 9(b), which is in good agreement with the sample shape. This result also proves the effectiveness of the method in the detection of complex targets. According to the fascia distribution characteristics of the limbs of the living body, the imaging algorithm can be used for tracking the position.

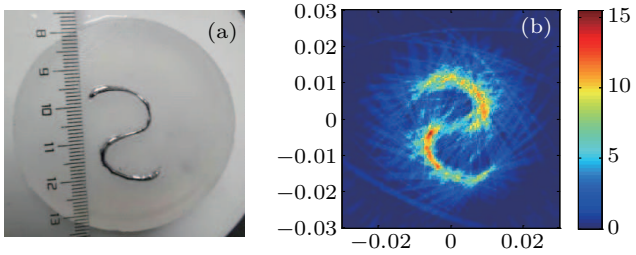


Fig. 9. Position imaging for plane curve sample, showing (a) sample and (b) position imaging.

4. Discussion and conclusions

In this paper, we propose a new method of studying the interstitial structure, which employs liquid metal to mark the interstitial fluid channel and image the liquid metal by MAT-MI to achieve the spatial reconstruction of the interstitial structure. The problem of MAT-MI for liquid metal in biological tissues is attributed to the spatial position imaging of liquid metal. By analyzing the characteristics of the waveform for the liquid metal under a certain size in MA detection, it is proposed that the envelope analysis method be used to solve the problem of data extraction when the multi-reflection waveforms of the MA signal overlap, and the liquid metal position imaging algorithm is designed based on the pixel matrix superposition method. Finally, the columnar liquid metal embedded in the gel is taken for sample, and multi-slice scanning is performed on circle path to collect the MAP signal for reconstructing the positional imaging, and the positional imaging of liquid metal by fewer sampling points is discussed. The results show that the envelope analysis method can effectively solve the problem of liquid metal position information extraction when sound pressure signals overlap, and positional imaging by superimposing the pixel matrix avoides the problem that inequality group has no solution due to unexpected data extraction caused by sampling data failure, which makes the imaging system have relatively high robustness and fault tolerance. Besides, the data extraction and position imaging methods proposed in this paper are equally applicable to the spatial position reconstruction of conductive objects of other

known materials. The MAT-MI technology with high conductivity fluid material as its detection object and tracer is an effective method of studying the circulation characteristics of interstitial fluid in biological tissues, which provides a new feasible method of studying the restricted space material transmission and information connectivity, and may provide new experimental basis for scientific explanation of TCM meridian theory. Furthermore, this position imaging method also has a certain application value in the position detection for known conductive material such as underground buried cable or metal pipe and other subjects.

In this study, the organism is simplified into a uniform fluid, and the liquid metal into a spatial linear structure without considering the influence of the complex structure of the organism. However, in the actual organism, there are bones and lung structures, as well as gas and other substances in the body cavity, the acoustic characteristics of which are quite different from soft tissues. In the future research, it is necessary to systematically study its influence on sound field propagation to improve the accuracy of signal extraction. The morphology of the interstitial structure in different parts of the body is quite different. For example, the interstitial of the extremities is approximately columnar or linear, the interstitial of the adventitia has a hollow tubular structure, and the interstitial of the trunk is closer to the sheet. Therefore, it is necessary to design different transducer arrays for the interstitial shape characteristics of different positions and the limb structure of the corresponding parts. Besides, under different physiological and pathological conditions of organisms, the fluid channel of the interstitial structure may appear to be ”bifurcation”, so it is necessary to consider the positional imaging problem of multiple liquid metal wires in the detection space. In addition, the spatial resolution of this imaging method is similar to the resolution of ultrasound imaging, which is about half the wavelength of the acoustic wave at the detection frequency. The detection target of the interstitial structure position is the target with a small size on a large space scale. Under this framework, the recognition efficiency of small size target needs improving. This is related to the strength of the excitation system and the sensitivity of the detection system, which can be achieved by optimizing the system parameters.

References

[1] Dennes P G 1992 *Angew. Chem. Int. Ed. Engl. (Nobel Lecture)* **31** 842
[2] Liao F L, Li M, Han D, *et al.* 2006 *Trends Pharmacol. Sci.* **27** 287
[3] Li H Y, Chen M, Yang J F, *et al,* 2012 *PLoS. One.* **7** e41395
[4] Benia P C, Wells R G and AboagyeB S 2018 *Sci. Rep-UK* **8** 4947
[5] Stecco C, Stern R, *et al.* 2011 *Surg. Radiol. Anat.* **33** 891
[6] Myers T W 2009 *Anatomy Trains: Myofascial Meridians for Manual and Movement Therapists*, 2nd edn. (New York: Churchill Livingstone) ISBN: 978-0-443-10283-7
[7] Kitamura S 2018 *Anat. Sci. Int.* **93** 1
[8] Adstrum S and Nicholson H 2019 *Clin. Anat.* **32** 862
[9] Shi X L, Zhu Y T, Dong H, *et al.* 2016 *Nano Res.* **9** 2097
[10] Moonen C, Vanzijl P, Frank J, *et al.* 1990 *Science* **250** 53
[11] Xu Y and He B 2005 *Phys. Med. Biol.* **50** 5175
[12] Li X, Yu K and He B 2016 *Phys. Med. Biol.* **61** R249
[13] Li X, Li X, Zhu S and He B 2009 *Med. Biol.* **54** 2667
[14] Ma Q and He B 2007 *Phys. Med. Biol.* **52** 5085
[15] Ma Q and He B 2008 *IEEE Trans. Biomed. Eng.* **55** 813
[16] Zhou L, Li X, Zhu S and He B 2011 *Phys. Med. Biol.* **56** 1967
[17] Li X, Xu Y and He B 2006 *J. Appl. Phys.* **99** 066112
[18] Sun X, Fang D, Zhang D and Ma Q 2013 *Med. Phys.* **40** 052902
[19] Li X and He B 2010 *IEEE Trans. Med. Imaging* **29** 1759
[20] Hu G, Cressman E and He B 2011 *Appl. Phys. Lett.* **98** 23703
[21] Mariappan L, Li X and He B 2011 *IEEE Trans. Biomed. Eng.* **58** 713
[22] Mariappan L and He B 2013 *IEEE Trans. Med. Imaging* **32** 619
[23] Guo G P, Ding H P, Ma Q Y, *et al.* 2017 *Chin. Phys. B* **26** 084301
[24] Mariappan L and He B 2013 *IEEE T. Med. Imaging* **32** 6410038
[25] Zhao X H, Liu G Q, Li Y H, *et al.* 2020 *J. Phys. D: Appl. Phys.* **53** 065401
[26] Li Z W, Li J, Li X P, *et al.* 2017 *Exp. Therm. Fluid Sci.* **82** 240
[27] Hu N Cao Y P, Han D, *et al.* 2018 *Nano. Res.* **11** 2265